Optical Materials 35 (2012) 25–28

Contents lists available at SciVerse ScienceDirect

Optical Materials

journal homepage: www.elsevier.com/locate/optmat

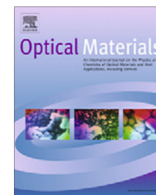

Planar single-crystal thin-films of YAG obtained by ion implantation and thermal exfoliation: Mechanical properties ☆

O. Gaathon [a,*], J.D. Adam [b], S.V. Krishnaswamy [b], J.W. Kysar [a], S. Bakhru [c], H. Bakhru [c], D.O. Welch [d], R.M. Osgood Jr. [a]

[a] Columbia University, New York, NY 10027, United States
[b] Northrop Grumman Systems Corporation, PO Box 1521, Baltimore, MD 21203, United States
[c] College of Nanoscale Science and Engineering, State University of New York at Albany, Albany, NY 12203, United States
[d] Department of Condensed Matter Physics and Materials Science, Brookhaven National Laboratory, Upton, NY 11973, United States

ARTICLE INFO

Article history:
Received 16 February 2012
Received in revised form 8 June 2012
Accepted 12 June 2012
Available online 20 July 2012

Keywords:
Yttrium Aluminum Garnet
Thin-film
Crystal Ion slicing
Ion implantation

ABSTRACT

We report on the fabrication of single-crystal thin films of Yttrium Aluminum Garnet (YAG, $Y_3Al_5O_{12}$) obtained by thermal exfoliation from bulk crystals after deep He-ion implantation. The film qualities and exfoliation process were determined by AFM, optical microscopy, SEM, optical profilometer and nanoindentation. The resulting films were subjected to annealing at ~1200 °C to relax the residual strain and film curvature that arose from the ion implantation process.

© 2012 Elsevier B.V. All rights reserved.

1. Introduction

Garnet crystals, such yttrium iron (YIG) and yttrium aluminum (YAG) garnet and related crystals, e.g. yttrium lanthanum fluoride (YLF) are essential to a wide variety of laser-, photonic-, and acoustic-based devices [1]. For integrated versions of these devices, thin films of the oxides are required. Despite important advances in the growth of single-crystal thin-films of YAG and other materials, the formation of fully crystal freestanding films with bulk-like properties has yet to be fully realized. One approach to fabricating these films is via ion-implantation-induced exfoliation. In this approach, high-energy ion-implantation of light ions is used to form a heavily implanted region below the surface of a target bulk single-crystal sample. This heavily implanted region forms the basis for film lift-off either through selective etching or other crystal separation approaches. In the past we have developed a technique called Crystal Ion Slicing (CIS) that is based on light ion implantation for exfoliation of thin films of complex oxides and other materials [2–10]. Thin-film devices that were obtained using this exfoliation technique were for applications in telecom and sensing [11–22]. In addition, TEM studies have been used to understand the atomic-scale physics of heavily implanted oxide crystals and its role in the exfoliation mechanism of various material systems [23–26].

The present work demonstrates fabrication of thin films of YAG for microsystem applications. Our approach uses ion-implantation followed by rapid heating in air to obtain the exfoliated sample. The fact that garnets such as YAG have a complex bonding structure with nearly equal surface energies for several low-index crystal planes causes the YAG crystal planes, to separate via conchoidal fracture; this makes the ion-induced microcleavage more challenging, as no clear cleavage plane is present. Further, the realization of large films requires control over the vertical thrust that is caused by implantation-induced strain. Our study demonstrates that relatively large high-quality films can be obtained and delineates the procedure needed to obtain planarized films, as well as the factors that control the size of free-standing films.

1.1. Experimental

Fabrication of the thin films followed a modified approach to that in crystal-ion-slicing (CIS) where light ions are implanted in the crystal creating a sacrificial layer that is more chemically active or has a different thermal expansion coefficient. Samples were prepared for exfoliation by implanting He^+ ions several microns below the surface of the crystal. Samples of 1 cm^2 were diced from a Czochralski-grown YAG wafer with ⟨001⟩ axis perpendicular to

☆ Any opinions, findings and conclusions or recommendations expressed in this material are those of the author(s) and do not necessarily reflect the views of the Department of Defense or the U.S. Government.

* Corresponding author.
E-mail address: og2126@columbia.edu (O. Gaathon).

0925-3467/$ - see front matter © 2012 Elsevier B.V. All rights reserved.
http://dx.doi.org/10.1016/j.optmat.2012.06.009

the surface. These samples were ion implanted (Dynamitron ion implanter) at energies of 1–4 MeV, with a projected ion range of 3–10 μm due to the ion-energy-dependent stopping range and straggle region of 160–410 nm, calculated using Stopping and Range of Ions in Matter (SRIM) simulation package [27]. The ion dose was varied between 2.5 and 8 $\times$ 10^{16} ions/cm^2. The samples were mounted on a water-cooled (17 °C) holder and were implanted 7° off the perpendicular direction.

In order to exfoliate the films, the samples were subjected to high-temperature ramping in a rapid thermal anneal (RTA) furnace (HEATPULSE 410) or a tube furnace (Thermolyne 21100) that was pre-heated to the desired temperature. In all cases, the implanted samples were introduced to the furnace at the required temperature for each experiment in a time interval of 4 s. After exfoliation, samples were removed from the heating device and allowed to cool to ambient temperature.

The surface of the films was analyzed by several methods: an optical profilometer (Wyko NT9100) and a long-working-distance, side-mounted optical microscope (custom built) were used to determine the long-range curvature of the films. For high-resolution investigation of the film's surface morphology, a scanning-electron microscope (SEM; Hitachi 5000 & LEO 1450) and an atomic-force microscope (AFM; Veeco MutiMode V) were used.

Mechanical properties of the implanted samples were measured using a nanoindenter (Agilent G200). Such a nanoindentor allows probing the mechanical properties as a function of depth on a nanometer length scale.

1.2. Results and Discussion

Samples were irradiated over a range of energies from 1.2–3.8 MeV such that a variety of films thicknesses could be obtained; this variation allowed us to examine the influence of film thickness on the exfoliation process. Fig. 1a–c shows side-view images obtained, via a scanning electron microscope (SEM), of implanted

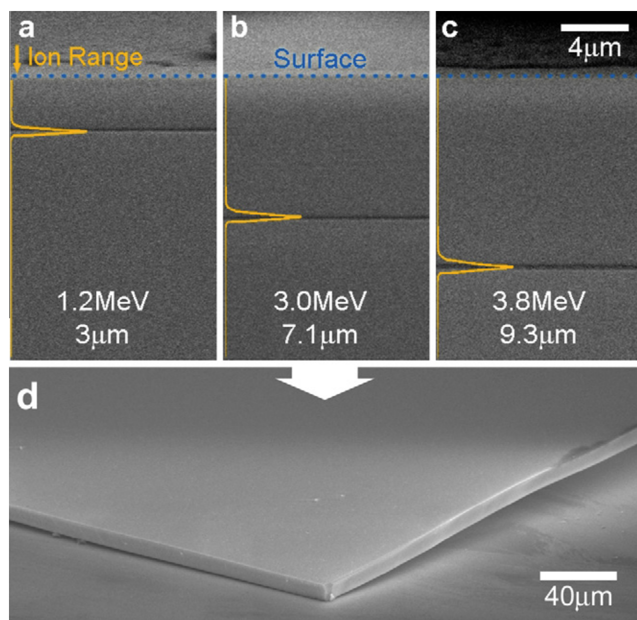

Fig. 1. (a–c) Scanning electron microscope (SEM) images of YAG crystal implanted at different energies (1.2 MeV, 3 Mev and 3.8 MeV). The doses for (a–c) are as follows: (a) (4 $\times$ 10^{16} ions/cm^2), (b) and (c) (5 $\times$ 10^{16} ions/cm^2). The overlaid light (yellow online) curve on the left of each inset is a TRIM calculation of He ions stopping range. (d) SEM image of exfoliated film of 3 MeV implanted YAG crystal on Si a wafer. (For interpretation of the references to color in this figure legend, the reader is referred to the web version of this article.)

YAG crystals at three different energies 1.2, 3 and 3.8 MeV. The crystals were lightly etched in phosphoric acid to indicate the narrow (a few hundred nm) stopping regions in each case. The yellow[1] curves in Fig. 1 shows the calculated projected ion range and straggle distance at each implantation energy for He in YAG crystal using SRIM. Earlier reports for other related material systems had shown that exfoliation occurred generally for doses of ~5 $\times$ 10^{16} ions/cm^2 for samples that were ~10 μm in thickness [8]. For the depth-dependent measurements, the dose was reduced as the implantation energy was lowered over the range given above from 5 $\times$ 10^{16} to 3.5 $\times$ 10^{16} ions/cm^2 because of the narrowing of the straggle region for lower energy. This procedure allowed us to maintain approximately the same He concentration in the implantation region at each implantation depth. A representative image in an SEM micrograph of the film can be seen in Fig. 1d. In this image, the implanted side of a 7 μm thin film is facing upward. Note that the films exhibit bowing due residual He near the back surface (top side in Fig. 1) as a result of the "tail" of the implant region.

A detailed atomic-scale mechanistic study of the slicing mechanism in other oxides, particularly $LiNbO_3$, have shown that He bubbles nucleate at implant-induced defects [24,28]. These defects then lead to the formation of a sheet of 'nanocleaves' in the highly-implanted crystal along the implant plane. The strong thermal gradients resulting from the presence of rapid oven heating provide localized stresses, which drive the exfoliation process. This mechanism can be characterized, as in many thermally activated processes [29], with an effective activation energy, E_a. This activation energy can be estimated using the usual Arrhenius expression,

$$E_A \propto K_B T \log(t_c) \tag{1}$$

where the time needed for exfoliation at temperature T is t_c and k_B is the Boltzmann constant. This thermally activated process was investigated by exposing samples to different exfoliation temperatures from 750 °C to 1200 °C and the thermal activation time was measured using a standard laboratory timepiece. The relation between slicing temperature and the time required to induce exfoliation, as indicated in Eq. (1), leads to an activation energy of 0.43 ± 0.04 eV. Experiments by Tong et al. [29] in Group IV semiconductors have shown that the exfoliation of a hydrogen-implanted sample has a characteristic activation energy, which for these elemental semiconductors is close to the bond energy of semiconductor. In our case, the material is more heavily implanted and thus a lower overall activation energy is reasonable.

Our nanoindentation measurements support the fact that implantation leads to a change in the mechanical properties in the implantation region. In this experiment, nanoindentation was used to probe the near-surface region of two different samples. Both samples were implanted with 1.2 MeV He ions at a dose of 3 $\times$ 10^{16} ions/cm^2. For the first experiment the sample was exfoliated and then nanoindentation was carried out on the *exfoliated* surface and compared to that on the surface of an unimplanted sample of YAG. The results showed that the straggle region has a Young's modulus that is repeatedly lower by at least 5% than that of the unimplanted sample, which is consistent with the crystal in the implantation region being damaged with point defects and dangling bonds [30]. In the second experiment, the Young's modulus of an implanted (unexfoliated) sample was characterized at different depths and compared with that of the unimplanted crystal. These measurements showed that the implanted sample had a decreased modulus beyond ~450 nm, which agrees with a decrease in the elastic modulus of the implanted region (~2.8 μm). For indentation depths significantly less than the straggle depth of the implanted samples, the Young's modulus was statistically

[1] For interpretation of color in Fig. 1, the reader is referred to the web version of this article.

identical to that of unimplanted samples. All measurements were repeated over 25 times to increase the statistical robustness of the results. Finally, we note that in all cases where there was a change in the modulus, it was very small, indicating that the mechanical properties of thin oxide films are generally unaffected beyond the heavily implanted region of the crystal.

Earlier experiments using implant-induced exfoliation on other oxide materials have shown that the residual interstitial He and any related defects, which remain after exfoliation, leads to bowing of the free-standing films. Thus in the case of $KTaO_3$ films it was earlier found that, after exfoliation via selective etching, the released samples exhibited an overall bending radius [31]. This bowing was attributed to residual nonuniform (thickness dependent) stress in the film that resulted from the tail of the implanted He distribution in the unetched portion of the thin-film sample. In microsystems applications, the lack of planarity in the films can cause difficulties in fabrication and patterning. In our YAG films, immediately following exfoliation, film bowing was measured via SEM or optical imaging, as is seen in Fig. 1.

Since bowing is attributable to interstitial He and related defects, we examined the effect of a high-temperature thermal-annealing schedule on the process. Such annealing is anticipated to drive out the implanted He and anneal out implant-induced lattice disorder and strain in the implantation region with the bulk thin-film crystal acting as a template. Thus an annealing treatment based on slow ramping and long annealing was used. Since annealing out of the strain field can be assisted by an externally applied oppositely directed strain field, in some cases the exfoliated film was loaded with a plate of sapphire. Both thermal exfoliation and high-temperature annealing were done in an ambient atmosphere. To quantify the bowing, measurements of surface curvature were made using a side view optical microscope and an optical profilometer (Wyko NT9100). The inset of Fig. 2 summarizes the results of measurements of the radius of curvature, R, as a function of annealing time at several temperatures. Using the well known Stony formula [32] one can express the average stress σ in the residual straggle region on the backside of the films as

$$\sigma = \frac{1}{6R}\frac{t_{YAG}^2}{t_{straggle^*}}\frac{E}{(1-\nu)}, \qquad (2)$$

where $t_{straggle*}$ is the thickness of the residual (remaining) straggle region, t_{YAG} the exfoliated film thickness, $t_{straggle*} \ll t_{YAG}$ the effective thickness of strained region, E the Young's modulus and ν is the Poisson ratio of YAG. Since the exact value of $t_{straggle*}$ after exfoliation is unknown, a precise value for σ in the residual straggle region is difficult to assess. Still, the ratio of σ to the initial stress σ_i, which is termed the stress ratio, for a given annealing temperature can be estimated, since this ratio is independent of $t_{straggle*}$. Fig. 2 shows the relative relaxation of stress in the film and in the residual straggle region for different annealing temperatures. Clearly, 1200 °C annealing is needed to fully relax and flatten the film. The data given in Fig. 2 clearly show the importance of stress in the exfoliated films.

Management of stress is also key to maintaining the integrity of the films for a given thermal exfoliation schedule. For example, without care in choosing the proper upper limit on dose, exfoliated films would fragment due to stress in the films from the exfoliation-induced strain. Thus clearly any strain in the film as a result of the ion implantation and the upward film thrust will be dependent on film implantation parameters and film thickness as well as the rapidity of the exfoliation process, which is dependent on the heating rate. Fig. 3 (right axis) shows a typical film-area dependence on dose for the 4 × 4 mm sample. It can be seen from the figure that a lower dose produced smaller film fragments because of the reduced strain during exfoliation. Note that for our sample size, it was found that in some exfoliation experiments samples with 4.5 and 5 × 10^{16} ions/cm^2 He, film fragments spanned the length of the samples and therefore their size was limited by the original bulk-sample dimensions. For example, our results show that as an example for a 4 × 4 mm sample, a dose of 4.5 × 10^{16} ions/cm^2 was determined to be optimal at our 3 MeV implantation energy.

In related experiments with unsupported films, i.e. those not having a handle wafer, it was found that there was also a correlation of exfoliation temperature and average film size. In particular, our experiments determined the optimum temperature to obtain the largest area films at each implantation energy. For example, in the case of 3 MeV ion energies, i.e. 7 μm thick films, 900 °C was determined to be the optimal temperature. For this temperature, large films (>4 × 4 mm) were obtained. In case of shallower implantation depths at 1.2 MeV (3 μm), a higher temperature was needed to realize large films. The insets in Fig. 4 shows typical optical microscope images of film fragmentation for a given thermal exfoliation temperature. The average time for the exfoliation to occur at each temperature is listed; Fig. 4 also shows the corresponding film size.

The experimental data shown in Fig. 4 along with prior work in ion exfoliation allow us to suggest a tentative mechanism for our results. In particular it has been previously found that via electron microscopy studies that implantation-induced interstitial defects,

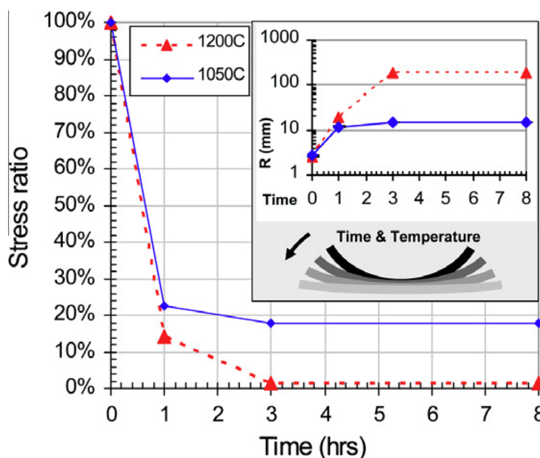

Fig. 2. Calculated stress ratio (see definition in text) of YAG films (from the initial stress state after exfoliation) as a function of annealing duration and temperature. Inset shows the measured radius of the curvature of the films versus time.

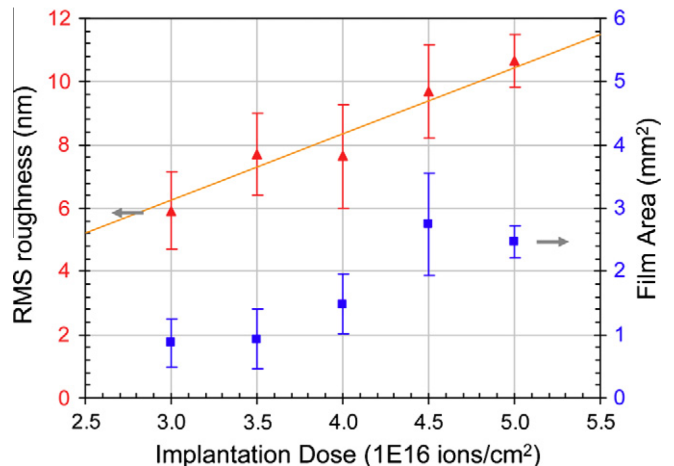

Fig. 3. RMS roughness of backside of the films (left – red online) and film area (right – blue online) for different implantation doses at implantation energy of 3 MeV. (For interpretation of the references to color in this figure legend, the reader is referred to the web version of this article.)

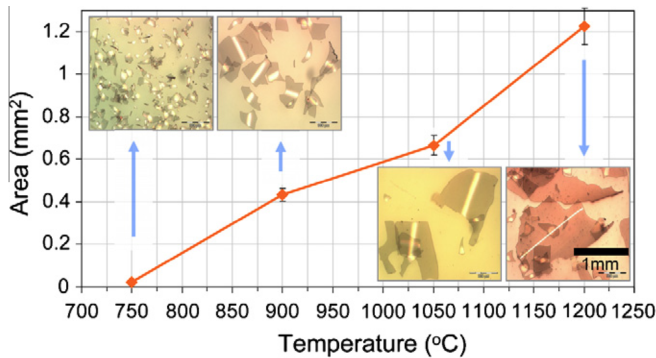

Fig. 4. Average area of film fragments for different exfoliation temperatures (implantation conditions: 1.2 MeV at 4×10^{16} ions/cm^2). Insets are optical microscope images of representative fragments.

i.e. bubbles, in other complex oxides have a size distribution within the plane of the straggle [24]. Upon annealing the average defect size increase with time and temperature via localized diffusion-enhanced mechanisms [25]. Further, exfoliation studies with the related system of Smart Cut in SOI have shown that, in that case, the critical defect size, at which exfoliation is initiated, is a function of the magnitude of the thermal stress; with higher temperatures requiring smaller critical defect sizes due to higher bubble pressure at higher temperature [33,34]. These experiments showed that at higher experimental annealing temperatures, the largest of the original as-implanted defects may exceed the critical defect size; in that case exfoliation could be initiated before significant void-size evolution occurs. Thus with rapid heating, exfoliation is governed by a few nucleation sites of low density, thus leading to the larger flakes as seen experimentally in our case. At lower but still elevated temperatures, Ostwald ripening and other diffusive mechanisms could operate locally to increase the defect sizes so that a greater number of defects exceed the critical defect size established for that temperature [35,36]. This would require more time and lead to a larger number of more closely spaced nucleation sites increasing the likelihood for microfractures to veer out of the straggle's plane and resulting in smaller exfoliated flakes. Clearly, additional TEM studies are needed to confirm this mechanistic scheme.

Finally, surface quality is also important in many applications. In order to evaluate the surface quality of the films after exfoliation, atomic force microscope (AFM) measurements of the surface morphology were made. Fig. 3 (left axis) summarizes the root-mean square (RMS) surface roughness of the backside of the films (that is the surface that is near to the implantation region) for doses ranging from 3–5 $\times 10^{16}$ ions/cm^2 at an implantation energy of 3 MeV. For each implantation dose, 4 $\times$ 4 mm samples were exfoliated at 900 °C. It was found that RMS roughness increased with implantation dose from 6 nm for 3×10^{16} ions/cm^2 to 10.5 nm for 5×10^{16} ions/cm^2. The data shows, within experimental error, a linear dependence of roughness with dose.

2. Conclusion

A new method for exfoliation of YAG films via ion implantation has been demonstrated and the mechanical properties of the film are characterized and optimized. The method enables fabrication of large-area (>5 mm^2), high quality films, with surface roughness below 10 nm. In order to reduce the implantation-induced strain (and the associated bowing) the films undergo a high temperature annealing at 1200 °C for several hours. The resulting films show a radius of curvature that is beyond 180 mm with a stress ratio of less than 1%.

Acknowledgments

This work was supported by the DARPA ART/CSSA program through The US Army Aviation & Missile Command under Contract No. W31P4Q-09-C-0528. Research was carried out, in part, at the Center for Functional Nanomaterials, Brookhaven National Laboratory, which is supported by the US Department of Energy, Office of Basic Energy Sciences, under Contract No. DE-AC02-98CH10886. J.W.K. acknowledges support from NSF CMMI-0927891 and AFOSR FA9550-09-1-0048. We would also like to thank Ryan Cooper for his assistance in this work.

References

[1] J.D. Adam, S.V. Krishnaswamy, S.H. Talisa, K.C.J. Yoo, Mag. Mag. Mater. 83 (1990) 419–424;
H. Kumagai, K. Adachi, M. Ezaki, K. Toyoda, M. Obara, Appl. Surf. Sci. 528 (1997) 109–110.
[2] A.M. Radojevic, M. Levy, R.M. Osgood Jr., A. Kumar, H. Bakhru, C. Tian, C. Evans, Appl. Phys. Lett. 74 (1999) 3197–3199.
[3] R. Liu, R. Guo, A.S. Bhalla, L.E. Cross, M. Levy, R.M. Osgood Jr., A. Kumar, H. Bakhru, Ferroelectr. 248 (2000) 45–56.
[4] R. Liu, R. Guo, A.S. Bhalla, L.E. Cross, M. Levy, R.M. Osgood Jr., Mater. Lett. 39 (1999) 264–267.
[5] M. Levy, R.M. Osgood Jr., A. Kumar, H. Bakhru, (AIP), pp. 6759–6761.
[6] M. Levy, R.M. Osgood Jr., R. Liu, L.E. Cross, G.S. Cargill Iii, A. Kumar, H. Bakhru, Appl. Phys. Lett. 73 (1998) 2293–2295.
[7] D. Scrymgeour, V. Gopalan, T. Haynes, Integr. Ferroelectr. 41 (2001) 35–42.
[8] M. Levy, R.M. Osgood Jr., A. Kumar, H. Bakhru, Appl. Phys. Lett. 71 (1997) 2617–2619.
[9] T. Izuhara, R.M. Osgood Jr., M. Levy, M.E. Reeves, Y.G. Wang, A.N. Roy, H. Bakhru, Appl. Phys. Lett. 80 (2002) 1046–1048.
[10] T. Izuhara, I.-L. Gheorma, R.M. Osgood Jr., A.N. Roy, H. Bakhru, Y.M. Tesfu, M.E. Reeves, Appl. Phys. Lett. 82 (2003) 616–618.
[11] D.W. Ward, E.R. Statz, K.A. Nelson, R.M. Roth, R.M. Osgood Jr., Appl. Phys. Lett. 86 (2005).
[12] A.R. Tarek, M. Levy, R.M. Osgood Jr., Appl. Phys. Lett. 76 (2000) 1407–1409.
[13] T.A. Ramadan, M. Levy, R.M. Osgood Jr., Appl. Phys. Lett. 76 (2000) 1407–1409.
[14] A.M. Radojevic, R.M. Osgood Jr., M. Levy, A. Kumar, H. Bakhru, IEEE Photonics Technol. Lett. 12 (2000) 1653–1655.
[15] A. Guarino, G. Poberaj, D. Rezzonico, R. Degl'Innocenti, P. Guenter, Nat. Photonics 1 (2007) 407–410.
[16] A.M. Radojevic, M. Levy, R.M. Osgood Jr., D.H. Jundt, A. Kumar, H. Bakhru, Opt. Lett. 25 (2000) 1034–1036.
[17] A.M. Radojevic, M. Levy, H. Kwak, R.M. Osgood Jr., Appl. Phys. Lett. 75 (1999) 2888–2890.
[18] M. Lilienblum, A. Ofan, A. Hoffmann, O. Gaathon, L. Vanamurthy, S. Bakhru, H. Bakhru, R.M. Osgood Jr., E. Soergel, Appl. Phys. Lett. 96 (2010).
[19] T. Izuhara, R. Roth, R.M. Osgood Jr., S. Bakhru, H. Bakhru, Electron. Lett. 39 (2003) 1118–1119.
[20] T. Gischkat, H. Hartung, F. Schrempel, E.-B. Kley, A. Tuennermann, W. Wesch, Microelectron. Eng. 86, (209) 910.
[21] P. Rabiei, W. Steier, Appl. Phys. Lett. 86 (2005) 161115.
[22] D. Djukic, G. Cerda-Pons, R.M. Roth, R.M. Osgood Jr., S. Bakhru, H. Bakhru, Appl. Phys. Lett. 90 (2007) 171116.
[23] R.M. Roth, D. Djukic, Y.S. Lee, R.M. Osgood Jr., S. Bakhru, B. Laulicht, K. Dunn, H. Bakhru, L. Wu, M. Huang, Appl. Phys. Lett. 89 (2006) 112906.
[24] A. Ofan, L. Zhang, O. Gaathon, S. Bakhru, H. Bakhru, Y. Zhu, D. Welch, R.M. Osgood Jr., Phys. Rev. B 82 (2010) 104113.
[25] A. Ofan, O. Gaathon, L. Vanamurthy, S. Bakhru, H. Bakhru, K. Evans-Lutterodt, R.M. Osgood Jr., Appl. Phys. Lett. 93 (2008) 181906.
[26] D. Djordje, M.R. Ryan, R.M. Osgood Jr., K. Evans-Lutterodt, B. Hassaram, B. Sasha, W. David, Appl. Phys. Lett. 91 (2007) 112908.
[27] J.F. Ziegler, Computer Code SRIM 2006.02, 2006, <http://www.srim.org>
[28] A. Klinger, M. Da-Silva, J. Soares, P. Fichter, L. Amaral, F. Zawislak, Nucl. Instrum. Methods Phys. Res. B 175 (2001) 394.
[29] Q.Y. Tong, K. Gutjahr, S. Hopfe, U. Gosele, T.H. Lee, Appl. Phys. Lett. 70 (1997) 1390–1392.
[30] D.J. Oliver, S. Ruffell, J.E. Bradby, J.S. Williams, M.V. Swain, P. Munroe, P.J. Simpson, Phys. Rev. B 80 (2009) 115210.
[31] M. Levy, R.M. Osgood Jr., A.S. Bhalla, R. Guo, L.E. Cross, A. Kumar, S. Sankaran, H. Bakhru, Appl. Phys. Lett. 77 (2000) 2124–2126.
[32] L.B. Freund, Solid State Thin Film Materials - Stress, Defect Formation and Surface Evolution, Cambridge University Press, 2004. pp. 90–4.
[33] L.B. Freund, Appl. Phys. Lett. 70 (1997) 3519–3521.
[34] F.J. Yang, Appl. Phys. 94 (2003) 1454–1457.
[35] P.D. Moran, M.J. Levy, Appl. Phys. 94 (2003) 3045–3050.
[36] J. Grisolia, G.B. Assayag, A. Claverie, B. Aspar, C. Lagahe, L. Laanab, Appl. Phys. Lett. 76 (2000) 852–854.